Atmos. Chem. Phys. Discuss., 8, 9209–9238, 2008
www.atmos-chem-phys-discuss.net/8/9209/2008/

Atmospheric Chemistry and Physics Discussions

Simulation of the climate impact of Mt. Pinatubo eruption using ECHAM5 – Part 1: Sensitivity to the modes of atmospheric circulation and boundary conditions

M. A. Thomas[1], C. Timmreck[1], M. A. Giorgetta[1], H.-F. Graf[2], and G. Stenchikov[3]

[1]Max-Planck Institute for Meteorology, Hamburg, Germany
[2]Center for Atmospheric Sciences, Cambridge University, UK
[3]Department of Environmental Sciences, Rutgers-The state university of NJ, USA

Received: 12 March 2008 – Accepted: 9 April 2008 – Published: 22 May 2008

Correspondence to: M. A. Thomas (manu.thomas@zmaw.de)

Published by Copernicus Publications on behalf of the European Geosciences Union.

Abstract

Large volcanic eruptions and their subsequent climate responses are relatively short-lived perturbations to the climate system. They provide an excellent opportunity to understand the response of the climate system to a global radiative forcing and to assess the ability of our climate models to simulate such large perturbations. The eruption of Mt. Pinatubo in Philippines in June 1991 was one of the strongest volcanic eruptions in the 20th century and this well observed eruption can serve as an important case study to understand the subsequent weather and climate changes. In this paper, the most comprehensive simulations to date of the climate impact of Mt. Pinatubo eruption are carried out with prescribed volcanic aerosols including observed SSTs, QBO and volcanically induced ozone anomalies. This is also the first attempt to include all the known factors for the simulation of such an experiment. Here, the climate response is evaluated under different boundary conditions including one at a time, thereby, investigating the radiative and dynamical responses to individual and combined forcings by observed SSTs, QBO and volcanic effects. Two ensembles of ten members each, for unperturbed and volcanically perturbed conditions were carried out using the middle atmosphere configuration of ECHAM5 model. Our results show that the pure aerosol response in lower stratospheric temperature is insensitive to the boundary conditions in the tropics and does not show some observed features which results from the boundary conditions. To simulate realistically the lower stratospheric temperature response, one must include all the known factors. The pure QBO and ocean responses are simulated consistent with earlier studies. The dynamical response manifested as the winter warming pattern is not simulated in the ensemble mean of the experiments. Our analysis also shows that the response to El Niño conditions is very strong in the model and that it partially masks the effects due to volcanic forcing.

1 Introduction

Large tropical volcanic eruptions can influence the global climate by reducing the amount of solar radiation reaching the Earth's surface (Dutton and Christy, 1992; Hansen et al., 1992; Stenchikov et al., 1998; Timmreck et al., 1999), lowering temperatures in the troposphere (Hansen et al., 1996; Kirchner et al., 1999; Robock, 2005; Stommel and Stommel, 1983), increasing temperatures in the tropical stratosphere (Timmreck et al., 1999; Stenchikov et al., 2002) and thereby changing atmospheric circulation patterns. The circulation in the lower atmosphere can be affected by short term stratospheric perturbations, for example, ozone changes (Rind et al., 1992; Grainger et al., 1993; Kodera, 1994; Randel et al., 1995; Timmreck et al., 2003). It is thus interesting to explore the various ways in which the stratospheric perturbations can influence the tropospheric circulation. Both models and observations point out to the fact that the troposphere and middle atmosphere are coupled through wave mean flow interaction, especially with respect to planetary Rossby waves (Sassi et al., 2004; Graf et al., 2007).

The variability in the stratosphere is mainly due to anomalous boundary forcings or natural internal variations. Natural internal variability arises from the non linearity of the dynamics of the circulation in the middle atmosphere. Boundary forcing arises from variations in the tropospheric forcing such as changes in radiative budget due to changes in atmospheric composition e.g. ozone depletion via volcanic aerosols/anthropogenic influences or re-distribution of tropical heat sources such as the El Niño-Southern Oscillation (ENSO) events. This can in turn give rise to changes in vertically propagating wave disturbances (Holton, 1982; Matsuno, 1970; Manzini et al., 2006). But, in the real world, where the circulation evolves under the continuous influence of a combination of factors, it is not simple to determine the responses to single influencing factors. For example, it is not possible to isolate the ENSO effects from other elements of natural variability if the signal is small and is strongly varying because of internal variability (Hamilton, 1993; Baldwin and Sullivan, 1995). However, it is possible to do so using a

numerical model, for example, where ENSO is the only specified source of variability in addition to internal model dynamics and other surface properties like snow cover or soil moisture, which are computed by the model.

The observed climate evolution following a major volcanic eruption has significant anomalies compared to climatology, indicating a link between the major volcanic eruptions and the climate anomalies. These have, however, occurred under additional influences of sea surface temperature (SST) anomalies (e.g. the major explosive volcanic eruptions of the last 50 years coincided with an El Niño.) and the specific phases of the Quasi-Biennial Oscillation (QBO) and possibly other influences. Hence while simulating this impact, one must consider all these interactions. In this paper, the generalized climatic response to Mt. Pinatubo eruption with different boundary conditions and forcings is examined. The response of the tropospheric and stratospheric circulation to individual and combined factors including volcanic forcing, varying SST boundary conditions and different states of the QBO are assessed. This is important as this gives us insights on how climate responds to the volcanic aerosol radiative forcing in which either one or more of the forcings such as the ocean state, QBO phase etc are included. The main scientific questions addressed in this paper are the following:

1. What is the pure effect of volcanic radiative forcing under different boundary conditions?
2. What is the response to combined influences of Mt. Pinatubo volcanic eruption and other boundary condition changes?

None of the simulations carried out so far included all the important factors together such as the effects of QBO, El Niño and volcanically induced ozone anomalies for the simulation of Mt. Pinatubo eruption. Hence, this study tries to simulate the response of this huge natural perturbation by including all the known factors and additionally, analyze the response to individual and combined forcings using the same model set up.

Mt. Pinatubo erupted on 15 June 1991 injecting 20 Mt of SO_2 into the lower stratosphere (Bluth et al., 1992) that was chemically transformed to sulfate aerosols, encir-

cling the globe in a month (McCormick and Veiga, 1992; Long and Stowe, 1994). The prominent dynamical impact that has generally been observed after explosive tropical eruptions is an anomalously positive phase of the Arctic Oscillation (Robock and Mao, 1992, 1995; Perlwitz and Graf, 1995). In this paper, we focus on the lower stratospheric temperature response and the boreal winter high latitude response in surface temperature and geopotential height at 30 hPa.

2 Model and datasets used

2.1 Model description

The most recent version of the fifth generation atmospheric general circulation model ECHAM5 developed at the Max Planck Institute for Meteorology, Hamburg (Special section "Climate models at the Max-Planck Institute for Meteorology" in Journal of Climate, 2006, 19, Issue-16, 3769-3987) is used at T42 horizontal resolution and with 39 vertical layers, topmost layer at 0.01 hPa (Manzini et al., 2006). Since radiative transfer is the major process linking the general circulation to volcanic aerosols in the stratosphere, the radiation schemes in both shortwave (SW) and longwave (LW) are mentioned briefly here. The SW radiative transfer scheme of ECHAM5 follows Fouquart and Bonnel (1980) and the LW radiative transfer follows the RRTM (Rapid Radiative Transfer Model) scheme (Mlawer et al., 1997) as implemented in cycle 23 release 1 of the IFS model of ECMWF (Morcrette et al., 1998). The number of spectral bands in the shortwave has been increased to 6 (0.185–4.00 μm) (Cagnazzo et al., 2007). Both the Near IR and the UV/VIS spectral range is resolved by three bands each to account better for the wavelength dependencies of optical properties of aerosols.
The radiative transfer calculations are made every two hours. Radiative heating rates are estimated at every 15 min time step based on the 2 hourly radiative flux calculations and the solar incidence that is calculated at every time step. The radiative transfer calculation requires profiles of active gases, aerosols, cloud water and ice and cloud

cover. Water vapor, cloud water and ice are prognostic variables. CO_2, CH_4, N_2O and CFCs are prescribed with a constant mixing ratio, and ozone is prescribed following the zonally averaged monthly climatology of Fortuin and Kelder (1998) which is based on the observation over a period 1980 - 1991. Aerosol distributions are prescribed following Tanre et al. (1984). This climatology distinguishes spatial distributions of sea, land, urban and desert aerosols and well mixed tropospheric and stratospheric background aerosols.

2.2 Datasets

For the volcanic aerosol forcing, Pinatubo aerosol data that have been compiled by G. Stenchikov from SAGE II (Stratospheric Aerosol and Gas Experiment) and UARS (Upper Atmosphere Research Satellite) satellite data for the specific model resolution is used. This data set makes use of the retrievals at 0.55 μm to calculate the aerosol parameters following the conventions used in Sato et al. (1993). The aerosol dataset consists of zonally averaged values of extinction cross section, single scattering albedo and asymmetry factor for two years following the Pinatubo eruption. The aerosol optical depth at 0.55 μm for two years after the eruption is shown in the Fig. 1. The spread of the volcanic aerosol cloud is clearly evident.
The ozone anomalies owing to Mt. Pinatubo eruption were compiled by G. Stenchikov (Stenchikov et al., 2002) from in-situ ozonesonde observations and are validated using TOMS (Total Ozone Mapping Spectrometer) column observations (Randel et al., 1995). To produce the ozone data set for our simulations, the monthly mean and zonal ozone anomalies are first interpolated to the model grid and then applied to the zonal mean ozone distribution used in ECHAM5. The zonally averaged ozone anomalies used in this study at 20 hPa for two years following the eruption is shown in the Fig. 2. There is a maximum ozone loss of up to 1.2 μg/g after July 1991 in the tropics. Positive ozone anomalies are visible in the equatorial region from Dec 1992 during the westerly QBO phase.

3 Experimental set up

The ensembles of perturbed and unperturbed runs carried out for two years following the Mt. Pinatubo eruption from June 1991–May 1993 with different boundary conditions are presented in Table 1. The perturbed runs include the zonally and monthly averaged prescribed volcanic aerosol distribution and volcanically induced ozone anomalies. The subscript "u" is used to denote the unperturbed runs and "p" for the corresponding perturbed runs. Runs are carried out with climatological SST (Clim_SST), observed SST (Obs_SST) and with boundary conditions combining observed SST and the observed QBO phase (O_QBO).

For each experimental set up of Table 1, an ensemble of 10 runs is carried out. In the perturbed experiments with climatological SST and sea ice conditions (C_p), the initial conditions are chosen arbitrarily from the a 15-year control run simulation with climatological SST and SIC distribution (C_u) after spin up. Thus, we have ten independent realizations. The ensemble mean response is calculated as an average difference of the ensemble mean, C_p of the perturbed runs and the unperturbed run mean, C_u.

Similarly, ensemble runs have been performed with observed SST and SIC as boundary conditions (from Atmospheric Model Intercomparison Project, Gates, 1992). Ten two-year experiments are carried out with Pinatubo aerosol forcing and ozone forcing (perturbed run) and without them (unperturbed run). For both cases, the initial conditions are taken from the 15 year control run made with climatological SST and SIC as boundary conditions and a spin up of 17 months using the observed lower boundary conditions of January 1990 to May 1991 is made before the beginning of the perturbed and unperturbed runs. The response in this case is calculated as a one-to-one difference of the ensemble means of the perturbed and the unperturbed ensembles, O_p and O_u respectively.

For the runs including the QBO, a similar procedure as above is adopted. In this case, a spin up of 17 months is carried out with observed SST and with the observed QBO phase. This experiment includes the 1991/1992 El Niño induced SST anomalies

that coincided with this eruption. To include the QBO forcing in this study, the zonal winds in the tropics are nudged towards the zonal wind observations at Singapore (Giorgetta and Bengtsson, 1999). The nudging is applied uniformly in a core domain and extends with decreasing nudging rate to the boundary of the domain. The latitudinal core domain specified for the study here is 7N-7S and the domain boundary is 10N-10S. In the vertical the core domain and the boundary is over the levels extending from 70 hPa to 10 hPa. The nudging rate is $(10\ \text{days})^{-1}$.

The ensemble runs can be analyzed in different ways as shown in Table 2 to obtain ensemble mean responses for specific forcing differences. The boxes show the differences between the corresponding perturbed ensemble (in the row) and the unperturbed control ensemble (in the column). For example, Aer1 is the ensemble mean difference C_p–C_u and Aer+O+QBO is the difference OQ_p–C_u. Hence, Aer1, Aer2 and Aer3 give the aerosol response under different boundary conditions. Aer1 gives the aerosol response under climatological SST as boundary conditions, Aer2 the aerosol response under observed SST as boundary conditions and Aer3 under both observed SST and QBO. The table also gives the responses to individual forcing differences of the ocean (O) and QBO (Q). The other responses discussed in this chapter are (1) the combined aerosol and ocean forcing (AO), (2) the combined aerosol and QBO forcing (AQ) and (3) the combined aerosol, ocean and QBO forcing (AOQ).

The main advantage of these experiments is that it is possible to isolate the effects of volcanic aerosol, the ocean and the QBO and also to assess their combined effects so as to better understand the observed responses.

4 Results and Discussion

A comparison of the different forcing experiments in simulating the tropical and high latitude response to the Mt. Pinatubo eruption is discussed. Here, we analyze the stratospheric temperature response that accounts for the radiative feedbacks. To estimate the dynamical feedbacks, this study also concentrates on the 30 hPa geopotential

and 2 m temperature anomalies in the high latitude for the two winters following the eruption.

4.1 Stratospheric temperature response

The SO_2 gas injected by volcanic eruptions into the stratosphere is chemically transformed to sulfate aerosol within a few weeks. Sulfate aerosol particles are purely scattering in the visible part of the solar spectrum, thus scattering the incoming solar radiation partially back to space, resulting in cooling of the Earth surface. In the near infrared (IR) and in the IR, sulfate aerosols are good absorbers, thus warming the aerosol layers significantly. The Pinatubo volcanic plume reached a maximum height of 40 km, with the bulk of aerosol centered around 25 km. Hence, in this section the simulation of the temperature response at 30 hPa to the Pinatubo aerosol forcing is discussed by means of the different forcing experiments.

As mentioned in the previous section, Aer1 and Aer2 give the aerosol responses for different SST boundary conditions (Table 1). In this case, Aer1 is the aerosol response for climatological SSTs, whereas Aer2 is the aerosol response where the boundary condition includes SST and ice of 1991–1993 including the effects of El Niño. In Fig. 3a,b, the tropical responses are similar in pattern, but the response is slightly higher with observed SST as boundary conditions, with a maximum of up to 3 K. The magnitude of the response is well simulated when compared to the observations (Fig. 3j). Both ENSO and QBO are prescribed as boundary conditions in the runs of Aer3 (Fig. 3c). The tropical response in Aer3 remains more or less the same as Aer1 and Aer2 simulations, different from the well structured observed anomalies. The response for Aer1, Aer2 and Aer3 in the latitudinal belt of 50 N–50 S is statistically significant at the 99% significance level from August 1991 to April 1993. The main point to be noted here is that the warming during the period January 1992–April 1992 in the Northern Hemisphere (NH) high latitudes in Aer3 corresponding to the weak polar vortex is consistent with observations (Fig. 3j) and is statistically significant at 95% confidence level, with temperatures reaching as high as 7 K, whereas, this signal is much weaker and is not

significant in Aer1 and Aer2. The large anomalies in the SH springtime high latitudes in the observations (Fig. 3j) are not simulated in these experiments.

Before analyzing the combined responses, it is important to analyze the ocean (O) and QBO (Q) alone ensemble differences to see whether the model reproduces the effect of El Niño and QBO circulation realistically.

Fig. 3d accounts for the effects of El Niño alone. ENSO signal propagates into the middle atmosphere by means of planetary Rossby waves and this propagation is strong when the stratospheric winds are westerly and peaks during boreal winter in the mid-latitudes (Garcia et al., 2006). Studies by Sassi et al. (2004); Manzini et al. (2006); Chen et al. (2003) have shown that during an El Niño event, the enhancement of vertical propagation and divergence of E-P flux cools the tropics and warms the high latitudes. Fig. 3d shows a similar pattern as in the literature except that the cooling in the tropics is less. The cooling is more evident in the 50 hPa temperature anomalies (not shown here).

Fig. 3e shows the QBO-related lower stratospheric temperature anomalies at 30 hPa. A cooling of about 1–2 K associated with the easterly phase of QBO is shown in the latitudinal belt from 15N-15S from June 1991 to June 1992 and warm anomalies in mid-latitudes. The opposite is seen during the westerly phase of QBO though the warming is only of about 0.5K. This cold bias of 1–1.5 K along the equator is because the reference model have no QBO and is therefore too cold at 30 hPa (refer Part-II of this paper for more details). The QBO signature in the stratospheric temperature can also be seen in the other responses with QBO (Fig. 3e,f,h and i) and is consistent with previous studies (Baldwin et al., 2001). The response to combined ocean and QBO forcings is shown in Fig. 3f and the responses are linear except in high latitudes, which means that the temperature response to combined ocean and QBO forcing is the sum of the temperature responses to single forcings by ocean and QBO.

The AO ensemble difference accounts for the effects of both aerosol and ocean (Fig. 3g). The maximum temperature anomaly of 2 K is simulated and here too, the responses are linear in the tropics.

Fig. 3h is the 30 hPa temperature response when both aerosol and QBO (AQ) effects are considered. The effect of easterly and westerly phase of QBO can be clearly seen. In the easterly phase, the AQ response shows a dual peak with relative maximum in the subtropics and a minimum at the equator and in the westerly phase, the AQ response shows a single equatorial peak. The significant warming beyond 60N during the winter of 1991/1992 and the cooling during the winter of 1992/1993 is not seen in the runs without the QBO and is consistent with observations. Comparing with the observed response as in Fig. 3j, the simulated response is most realistic when A, O and Q forcings are included (Fig. 3i). There is not much difference between the AQ and AOQ, except that the high latitude response in first boreal winter is much stronger in AOQ. Though the NH high latitude response is realistically simulated, it has to be noted that large discrepancies exist in the southern hemisphere high latitudes in all the model simulations. Hence, to simulate the pattern and the magnitude of the observed lower stratospheric temperature anomalies realistically, it is best to include all three forcings, namely, volcanic radiative forcing, observed SST/ice and the correct QBO phase.

4.2 Geopotential height response at 30 hPa

In the two winters following the major eruptions, an anomalously positive AO index (Thompson et al., 1998; Baldwin and Dunkerton, 1999) is observed. Fig. 5a–r shows the 30 hPa geopotential height anomaly as a representative of the strength of the polar vortex for all the forcing experiments considered here and Fig. 5s,t shows the observed response calculated from ERA-40 Re-analysis data after Mt. Pinatubo eruption. Of which, the left column is the response for the first winter and the right column is the response for the second winter following the eruption. In both winters, the aerosol response simulated under climatological SST as boundary conditions (Fig. 5a,b) does not capture the magnitude and spatial pattern of the polar vortex (refer Fig. 5s,t). However, under observed SST as boundary conditions (Fig. 5c,d), the aerosol response shows an anomalously strong stratospheric polar vortex in the second winter that is

consistent with the observations, but the anomaly is weaker and not statistically significant. The geopotential height anomaly reaches –100 m

The ENSO effect on the winter circulation is shown in Fig. 5g,h. A dipole structure is seen with above normal geopotential height anomalies over northern N. America and Russia and below normal anomalies over northern Atlantic and Europe during the first winter, whereas in the second winter, the dipole is shifted clockwise, with above normal anomalies over the poles and Russia and below normal geopotential heights over northern Atlantic. During a warm ENSO, enhanced wave propagation in boreal winter disturbs the polar vortex (Sassi et al., 2004; Manzini et al., 2006).

In the westerly phase of QBO the polar vortex is expected to be anomalously strong and in the easterly phase anomalously weak (Holton and Tan, 1980, 1982) in the absence of the aerosol effects. This is evident in the QBO experiment, where the QBO is the only source of variability (Fig. 5i,j). Fig. 5j shows that the geopotential height anomalies at high latitudes is lower reaching a minimum value –140 m and is surrounded by above normal anomalies in the second winter when QBO is in its westerly phase.

The combined effects of ENSO and QBO (OQ) do not simulate a strong vortex in neither of the two winters (Fig. 5k,l). This is because, during the first winter, neither ENSO nor the easterly phase of QBO favors an anomalously strong polar vortex. But, during the second winter, with the ENSO effects relatively weak and with QBO in its westerly shear, the model still cannot produce a strong polar vortex, reflecting the non-linearity in the way QBO modulates the circulation. A dipole structure is observed with low values over Europe, Russia and the northern Atlantic and high values over Canada in the first winter and the opposite is observed in the second winter.

The polar vortex is disturbed for the combined aerosol and ocean (AO) forcing in both winters (Fig. 5m,n). The same is seen for the combined aerosol and QBO (AQ) forcing in the first winter (Fig. 5o). However, in the second winter of AQ response, the polar vortex is more stable (Fig. 5p). This may be because, the westerly shear of the QBO favors a polar vortex with values reaching as low as 220 m. With all the effects included, the model simulates the deepening of the geopotential height anomaly in the second

winter, though the magnitudes are relatively weak (around –100 m). It should be noted that the polar vortex was much weaker after the first winter following Mt. Pinatubo eruption compared to the second winter when the vortex was deeper (Fig. 5s,t) . This study suggests that there is significant non-linearity between aerosol and QBO effects and the strengthening of the polar vortex is more effective when the QBO is in the westerly phase.

4.3 2 m temperature response

Stratospheric sulfate aerosol particles from strong tropical volcanic eruptions produce significant warming in the lower equatorial stratosphere thereby increasing the equator to pole temperature gradient in the lower stratosphere of the winter hemisphere. This forces a positive phase of the Arctic Oscillation during northern winter and as a dynamical response produces a winter warming pattern at the surface (Stenchikov et al., 2002). This pattern is manifested as a prominent warming over Northern and Eastern Europe and Siberia and cooling over Greenland and Middle East. This is presented in the Fig. 4s and t respectively for the first and second winters following the Mt. Pinatubo eruption, where warming of up to 3–5 K are observed over N. Europe and Siberia and cooling up to –5 K is observed over Greenland and up to –2 K over the Middle East. This feature is typical of low latitude volcanic eruptions of the explosive type (Oman et al., 2005).

Figure 4a–r show the ensemble mean surface temperature anomalies for two winters following the Pinatubo eruption. The shading in the figures corresponds to the level of significance. Areas with significance level above 95% are heavily shaded and above 90% lightly shaded.

For the two winters, the warming over northern Europe and Siberia is weakly simulated by the model with climatological SST as boundary conditions (Aer1) (Fig. 4a,b) and is shifted further north, but the anomalies are not significant. The cooling over the Middle East is simulated by the model in the Aer1 experiments reasonably well, though the

magnitudes are over-estimated. With observed SST as boundary conditions (Fig. 4c), the aerosol response cannot reproduce the volcanic winter pattern during the first winter. This may be because of El Niño that is present during the first winter and the signal is stronger than the effects due to the volcanic aerosols. However, the volcanic winter pattern is weakly simulated in the second winter (Fig. 4d), but they are not statistically significant. With both observed SST and QBO effects, the aerosol response show significant cooling over Eurasia. Hence, we can conclude that model is not able to reproduce the observed volcanic winter pattern in the ensemble means with respect to the volcanic radiative forcing alone under the set of boundary conditions considered here.

The individual responses to El Niño SST in the winter circulation is shown in Fig. 4g,h. The warm anomalies associated with El Niño over the Eastern Pacific are clearly seen in the ocean response alone experiments (Fig. 4g,h) which is expected as the SST in this case is prescribed from observations. The ENSO-related warming over central and northern North America during the winter of 1991/1992 is also well simulated by the model. However, statistically significant above normal temperatures are observed beyond north of 60N and cooling over Middle East and parts of Europe and China for both the winters following the eruption. These anomalies are not seen in the observed temperature anomalies in El Niño winters excluding volcanic eruptions (not shown). However, in these experiments, it can only be attributed to the observed SST differences between the observed period and the climatology or to internal variability. It has to be noted that these anomalies are evident in the second winter, when the El Niño effects are negligible.

The QBO effects on the winter circulation of 1991/1992 and 1992/1993 are presented in Fig. 4i,j respectively. Significant warming over Europe, parts of Russia and over Eastern China and cooling over northern North America, Canada and Greenland is simulated for the two winters. However, the warming is slightly weaker in the second winter. The combined ocean and QBO effects (Fig. 4k–l) produces the spatial patterns to some extend in both the winters and is closest to the observed winter warming, but

the magnitude of the anomalies are less than the observed and there is a northward shift.

The AO experiment that accounts for the effects of both aerosol and the state of the ocean for the two winters are shown in Fig. 4m,n. The patterns associated with ENSO during the first winter is clearly seen in the figures and the interactions between aerosol and ocean seems to be minimal. Comparing the AO-related response with the ocean response, the only difference is that the warming over Eurasia in the first winter is more pronounced in the AO response and colder temperatures are observed over Greenland in the second winter in the AO response which is typical of volcanic winters. This may be because the ocean response is more stronger in the model, thereby, over-riding the effects due to volcanic eruptions.The combined effects of aerosol and QBO in the AQ experiment (Fig. 4o,p) do not reproduce the observed volcanic winter patterns in both the winters. Even in the case where all effects, aerosol, ENSO and QBO are included (Fig. 4q,r), the pattern is shifted poleward.

The ensemble mean responses to individual and combined forcings for two NH winters cannot reproduce the observed warming, though the cooling is simulated fairly well by some of the forcing experiments. One of the possible reasons can be that the model may not have sufficient vertical resolution in the upper troposphere and lower stratosphere to resolve the interactions between troposphere and stratosphere accurately. Our analysis also shows that the ENSO signal is dominating and modulated by QBO, partly masks the effects due to volcanic forcing. Another reason would be that zonally averaged volcanic forcing and volcanically induced ozone anomalies are used in the model simulations. The omission of the zonal asymmetric component of volcanic forcing and ozone forcing may produce differences in the response. It is shown that the zonally asymmetric component of ozone has an effect on the stratospheric temperature and planetary wave propagation (Gabriel et al., 2007). Also, the recent IPCC models used for the same analysis (Stenchikov et al., 2006) could not reproduce this dynamical response. Although in the mean response, the model cannot simulate the dynamical response correctly, it should be noted that about 30% of the individual ensemble mem-

bers for some of the forcing experiments do simulate this response realistically.

5 Conclusions

In this paper, the generalized climatic response to the Mt. Pinatubo eruption is investigated. The response of the tropospheric and stratospheric circulation to individual and combined factors such as volcanic forcing, varying SST boundary conditions and different states of QBO are assessed. This study is important as it provides insights on how the climate responds to the volcanic forcing when either one or more of the boundary conditions are included. To evaluate how well the model simulates these observed impacts, ensembles of perturbed and unperturbed runs are carried out using the middle atmosphere version of ECHAM5 with different boundary conditions and the differences between the several combinations of perturbed and unperturbed runs give the individual and combined responses due to volcanic forcing, El Niño and QBO effects. So, the ensemble mean differences gives an idea on how different the responses would be if El Niño was not present or if only the volcanic forcing exists, which otherwise, would have been possible to estimate without these sets of experiments.

Our results can be summarized as follows:

1. The lower stratospheric temperature response to the volcanic forcing in both the tropics and the winter response in the NH high latitudes is simulated realistically when all the known factors such as the volcanically induced ozone anomalies, the observed ocean state and the QBO effects are included.
2. The tropical stratospheric temperature response is linear with respect to the effects of single forcings.
3. The pure aerosol response in the lower stratospheric temperature is insensitive to the boundary conditions.

4. The signature of the easterly and westerly phases of the QBO in stratospheric temperature is simulated realistically in the pure QBO forcing experiments.

5. The ensemble mean effects of individual and combined forcings for two winters following the eruption could not reproduce the warming over northern and Eastern Europe and Siberia and the cooling over Middle East and Greenland, though this pattern was simulated by 30% of the ensemble members.

6. Our analysis shows that the response of the atmosphere to the ocean is very strong in the model. It overrides the effects due to the volcanic forcing. The ocean-related response is evident in the combined responses such as AO, OQ and AOQ and this explains the dominance over other effects.

7. The aerosol forcing from explosive volcanic eruptions tends to strengthen the polar vortex irrespective of the QBO phase. The model tries to simulate the polar vortex deepening in the second winter, when the QBO is in its westerly phase in Aer3 response and the combined responses of AQ and AOQ, though the simulated response is weaker compared to the observations. The vortex is disturbed during the first winters due to the enhanced wave propagation in boreal winter that in turn disturbs the vortex.

The model simulates the radiative response correctly, but, the simulation of the dynamical response still remains a challenge, even in the IPCC models. Further investigations are necessary to improve the models ability to simulate the dynamical response after large volcanic eruptions.

Acknowledgements. Computations were done at the German Climate Computer Center (DKRZ). C. T. is supported by the German Science Foundation DFG grant TI 344/1-1. G. S. was supported by NSF grant ATM-0351280 and NASA grant NNG05GB06G. We would also like to acknowledge ERA-40 project for the data used in this study that was obtained from the ECMWF data server.

References

Baldwin, M. P. and O'Sullivan, D.: Stratospheric effects of ENSO related tropospheric circulation anomalies, J. Clim., 8, 649–667,1995. 9211

Baldwin, M. P. and Dunkerton, T. J.: Propagation of the Arctic Oscillation from the stratosphere to the troposphere, J. Geophys. Res., 104, 30 937–30 946, 1999. 9219

Baldwin, M. P., Gray, L. J., Dunkerton, T. J., Hamilton, K., Haynes, P. H., Randel, W. J., Holton, J. R., Alexander, M. J., Hiorta, I., Horinouchi, T., Jones, D. B. A., Kinnersley, J. S., Marquardt, C., Sato, K., and Takahashi, M.: The quasi-biennial oscillation, J. Geophys. Res., 104, 30 937–30 946, 2001. 9218

Bluth, G. J. S., Doiron, S. D., Schnetzler, S. C., Krueger, A. J., and Walter, L. S.: Global tracking of the SO2 clouds from the June 1991 Mount Pinatubo eruptions, Geophys.Res. Lett., 19, 151–154, 1992. 9212

Cagnazzo, C., Manzini, E., Giorgetta, M. A., and De Forster, P. M.: Impact of an improved radiation scheme in the MAECHAM5 general circulation model, Atmos. Chem. Phys., 7, 2503–2515, 2007, http://www.atmos-chem-phys.net/7/2503/2007/. 9213

Chen, W., M. Takahashi and H.-F. Graf: Interannual variations of stationary planetary wave activity in the northern winter troposphere and stratosphere and their relations to NAM and SST, J. Geophys. Res., 108, 4797, doi:10.1029/2003JD003834, 2003. 9218

Dutton, E. G. and Christy, J. R.: Solar radiative forcing at selected locations and evidence for global lower tropospheric cooling following the eruption of El Chichón and Pinatubo", Geophys. Res. Lett., 19, 2313–2316, 1992. 9211

Fortuin, J. P. F. and Kelder, H.: An ozone climatology based on ozonesonde and satellite measurements, J. Geophys. Res., 103, 31 709–31 734, 1998. 9214

Fouquart, Y. and Bonnel, B.: Computations of solar heating of the earth's atmosphere: A new parameterization, Contrib. Atmos. Phys., 53, 35–62, 1980. 9213

Gabriel, A., Peters, D., Kirchner, I., and Graf, H.-F.: Effect of zonally asymmetric ozone on stratospheric temperature and planetary wave propagation, Geophys. Res. Lett., 34, L06807, doi:10.1029/2006GL028998, 2007. 9223

Garcia-Herrera, R., Calvo, N., Garcia, R. R., and Giorgetta, M. A.: Propagation of ENSO temperature signals into the middle atmosphere: A comparison of two general circulation models and ERA-40 reanalysis data, J. Geophys. Res., 111, D06101, doi:10.1029/2005JD006061,

2006. 9218
Gates, W. L.: AMIP: The Atmospheric Model Intercomparison Project, Bull. Amer. Met. Soc., 73, 1962–1970, 1992. 9215
Giorgetta, M. and Bengtsson, L.: The potential role of the quasi-biennial oscillation in the stratosphere-troposphere exchange as found in water vapor in general circulation model experiments, J. Geophys. Res., 104, 6003–6019, 1999. 9216
Graf, H.-F., Li, Q., and Giorgetta, M. A.: Volcanic effects of climate: Revisiting the mechanisms, Atmos. Chem. Phys., 7, 4503–4511, 2007, http://www.atmos-chem-phys.net/7/4503/2007/. 9211
Grainger, R. G., Lambert, A., Taylor, F. W., Remedios, J. J., Rogers, C. D., and Corney, M.: Infrared absorption by volcanic stratospheric aerosols observed by ISAMS, Geophys. Res. Lett., 20, 1287–1290, 1993. 9211
Hamilton, K.: An examination of observed Southern Oscillation effects in the Northern Hemisphere stratosphere, J. Atmos. Sci., 50, 3468–3473, 1993. 9211
Hansen, J., Lacis, A., Ruedy, R., and Sato, M.: Potential climate impact of Mt. Pinatubo eruption, Geophys. Res, Lett., 19, 215–218, 1992. 9211
Hansen, J., Ruedy, R., Sato, M., and Reynolds, R.: Global surface air temperature in 1995, return to pre-Pinatubo level, Geophys. Res. Lett., 23, 1665–1668, 1996. 9211
Holton, J. R. and Tan, H.-C.: The influence of the equatorial quasi-biennial oscillation on the global circulation at 50 mb, J. Atmos. Sci., 37, 2200–2208, 1980. 9220
Holton, J. R. and Tan, H.-C.: The quasi biennial oscillation in the Northern Hemisphere lower stratosphere, J. Meteo. Soc. Japan, 60, 140–148, 1982. 9220
Holton, J. R.: The role of gravity waves induced drag and diffusion on the momentum budget of the mesosphere, J. Atmos. Sci., 40, 2497–2507, 1982. 9211
Kirchner, I., Stenchikov, G. L., Graf, H.-F., Robock, A., and Antuna, J. C.: Climate model simulation of winter warming, summer cooling following the 1991 Mount Pinatubo volcanic eruption, J. Geophys. Res., 104, 19039–19055, 1999. 9211
Kodera, K.: Influence of volcanic eruptions on the troposphere through stratospheric dynamical processes in the northern hemisphere winter, J. Geophys. Res., 99, 1273–1282, 1994. 9211
Long, C. S. and Stowe, L. L.: Using the NOAA/AVHRR to study stratospheric aerosol optical thicknesses following Mt. Pinatubo eruption, Geophys. Res. Lett., 21, 2215–2218, 1994. 9213
Manzini, E., Giorgetta, M. A., Esch, M., Kornblueh, L., and Roeckner, E.: The influence of sea

surface temperatures on the northern winter stratosphere: Ensemble simulations with the MAECHAM5 model, J. Clim., 19, 3863–3881, 2006. 9211, 9213, 9218, 9220
Matsuno, T.: Vertical propagation of stationary planetary waves in the winter Northern Hemisphere, J. Atmos. Sci., 27, 871–883, 1970. 9211
McCormick, M. P. and Veiga, R. E.: SAGE II measurements of early Pinatubo aerosols, Geophys. Res, Lett., 19, 155–158, 1992. 9213
Mlawer, E. J., Taubman, S., Brown, P. D., Iacono, M. J., and Clough, S. A.: Radiative transfer for inhomogeneous atmospheres: RRTM, a validated correlated-k model for the longwave, J. Geophys. Res., 102, 16 663–16 682, 1997. 9213
Morcrette, J. J., Clough, S. A., Mlawer, E. J., and Iacono, M. J.: Impact of a validated radiative transfer scheme, RRTM on the ECMWF model climate, 10-day forecasts, Technical Memorandum, ECMWF, Reading, UK, 252, 1998. 9213
Oman, L., Robock, A., Stenchikov, G., Schmidt, G. A., and Ruedy, R.: Climatic response to high latitude volcanic eruptions, J. Geophys. Res., 110, D13103, doi:10.1029/2004JD005487, 2005. 9221
Perlwitz, J. and Graf, H.-F.: The statistical connection between tropospheric and stratospheric circulation of the Northern Hemisphere in winter, J. Clim., 8, 2281–2295, 1995. 9213
Ramachandran, S., V. Ramaswamy, G. L. Stenchikov and A. Robock: Radiative impact of the Mount Pinatubo volcanic eruption: Lower stratospheric response, J. Geophys. Res., 105, 24409–24429, 2000.
Randel, W. J., Wu, F., Russell III, J. M., Waters, J. W., and Froidevaux, L.: Ozone, temperature changes in the stratosphere following the eruption of Mount Pinatubo, J. Geophys. Res., 100, 16753–16764, 1995. 9211, 9214
Rind, D., Balachandran, N. K., and Suozzo, R.: Climate change and the middle atmosphere, Part II, The impact of volcanic aerosols, J. Clim., 5, 189–208, 1992. 9211
Robock, A. and Mao, J.: Winter warming from large volcanic eruptions, Geophys. Res. Lett., 19, 2405–2408, 1992. 9213
Robock, A. and Mao, J.: The volcanic signal in surface temperature observations, J. Clim., 8, 1086–1103, 1995. 9213
Robock, A.: Cooling following large volcanic eruptions corrected for the effect of diffuse radiation on tree rings, Geophys. Res. Lett., 32, L06702, doi:10.1029/2004GL022116, 2005. 9211
Sassi, F., Kinnison, D., Boville, B. A., Garcia, R. R., and Roble, R.: Effect of El Niño-Southern

Oscillation on the dynamical, thermal, chemical structure of the middle atmosphere, J. Geophys. Res., 109, D17108, doi:10.1029/2003JD004434, 2004. 9211, 9218, 9220

Sato, M., Hansen, J. E., McCormick, M. P., and Pollack, J. B.: Stratospheric aerosol optical depths, 1850–1990, J. Geophys. Res., 98, 22 987–22 994, 1993. 9214

Stenchikov, G., Kirchner, I., Robock, A., Graf, H.-F., Antuna, J. C., Grainger, R. G., Lambert, A., and Thomason, L.: Radiative forcing from the 1991 Mount Pinatubo volcanic eruption, J. Geophys. Res., 103, 13 837–13 857, 1998. 9211

Stenchikov, G., A. Robock, V. Ramaswamy, M. D. Schwarzkopf, K. Hamilton and S. Ramachandran: Arctic Oscillation response to the 1991 Mount Pinatubo eruption: Effects of volcanic aerosols, ozone depletion, J. Geophys. Res., 107, 1-16, 2002. 9211, 9214, 9221

Stenchikov, G., Hamilton, K., Stouffer, R. J., Robock, A., Ramaswamy, V., Santer, B., and Graf, H.-F.: Arctic Oscillation response to volcanic eruptions in the IPCC AR4 climate models, J. Geophys. Res., 111, D07107, doi:10.1029/2005JD006286, 2006. 9223

Stommel, H. and Stommel, E.: Volcano Weather – The story of 1816, the Year Without Summer, Seven Seas Press, Newport, R. I., 177, 1983. 9211

Tanre, D., Geleyn, J.-F. and Slingo, J. M.: First results of the introduction of an advanced aerosol-radiation interaction in the ECMWF low resolution global model, In Aerosols and Their Climatic Effects, 133-177, 1984. 9214

Thompson, D. W. J. and Wallace, J. M.: The Arctic Oscillation signature in the wintertime geopotential height and temperature fields, Geophys. Res. Lett., 25, 1297–1300, 1998. 9219

Timmreck, C., Graf, H-F., and Kirchner, I.: A one and a half year interactive MAECHAM4 simulation of Mount Pinatubo aerosol, J. Geophys. Res., 104, 9337–9359,1999. 9211

Timmreck, C., Graf, H.-F., and Steil, B.: Aerosol chemistry interactions after the Mt. Pinatubo eruption, Volcanism and the Earth's Atmosphere, AGU Monograph, 139, 213–225, 2003. 9211

Table 1. Perturbed and unperturbed ensemble experiments. The subscript "u" is used to denote the unperturbed runs and "p" is used for perturbed runs. C stands for climatological SST; O stands for observed SST; Q for QBO.

Experiments	Clim_SST (C)	Obs_SST (O)	O_QBO (OQ)
Unperturbed runs	C_u	O_u	OQ_u
Perturbed runs	C_p	O_p	OQ_p

Table 2. Ensemble mean differences between perturbed and unperturbed runs. The text in bold are the difference between the corresponding perturbed runs and unperturbed control runs.

Unperturbed runs			Perturbed runs		
O_u	C_u	—	C_p	O_p	OQ_p
		C_u	Aer1	Aer+O	Aer+O+QBO
	Ocean (O)	O_u		Aer2	Aer+QBO (AQ)
QBO	QBO+O (Q)	OQ_u (OQ)			Aer3

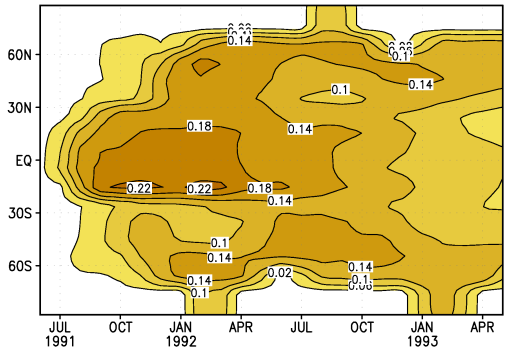

Fig. 1. Zonally averaged Pinatubo aerosol optical depth at 0.55 μm for two years after the eruption.

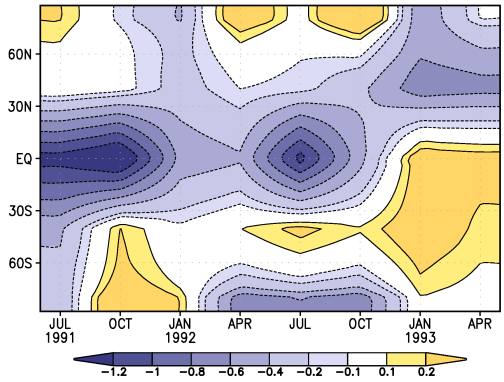

Fig. 2. Zonally averaged volcanically induced ozone anomalies at 20 hPa in (μg/g) for two years after the eruption.

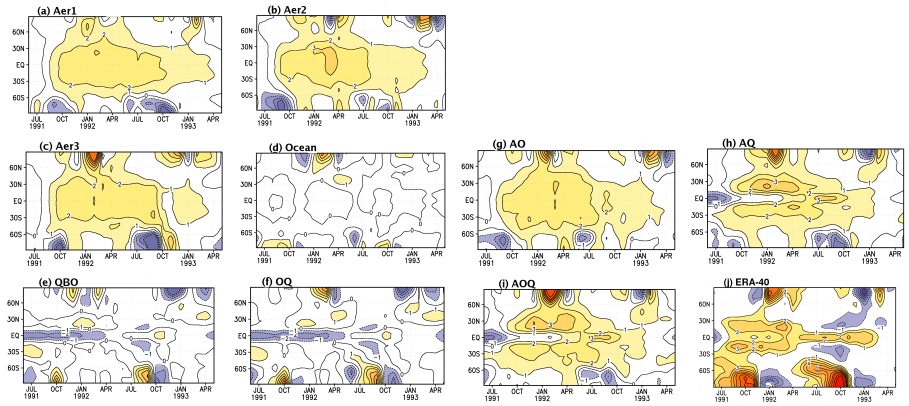

Fig. 3. Lower stratospheric temperature anomalies at 30 hPa (K) for **(a)** Aer1 **(b)** Aer2 **(c)** Aer3 **(d)** ocean response **(e)** QBO response **(f)** combined ocean and QBO – OQ **(g)** combined aerosol and ocean – AO **(h)** combined aerosol and QBO – AQ **(i)** combined aerosol, ocean and QBO – AOQ **(j)** ERA-40.

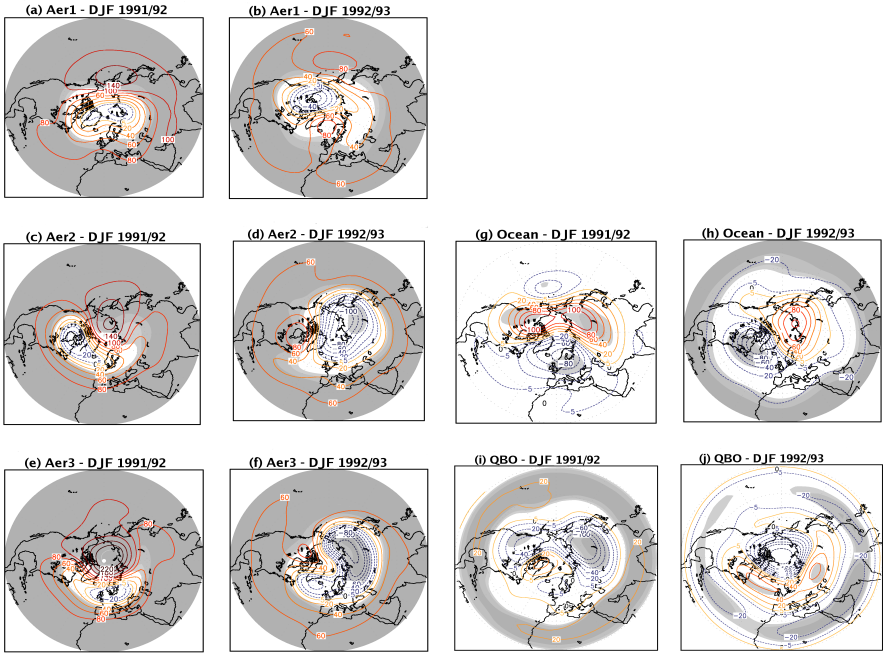

Fig. 4. Geopotential height anomalies at 30 hPa (m) for Aer1 (**a** and **b**); Aer2 (**c** and **d**); Aer3 (**e** and **f**); ocean response (**g** and **h**); qbo response (**i** and **j**); combined ocean and qbo (OQ) (**k** and **l**); combined aerosol and ocean (AO) (**m** and **n**); combined aerosol and QBO (AQ) (**o** and **p**); combined aerosol, ocean and QBO (AOQ) (**q** and **r**); for DJF 1991/1992 (left column) and DJF 1992/1993 (right column). Heavily shaded areas are significant at 99% level, lightly shaded at 90% significance level. Observed 30 hPa geopotential height response from ERA-40 (m) for DJF 1991/1992 (**s**) and DJF 1992/1993 (**t**).

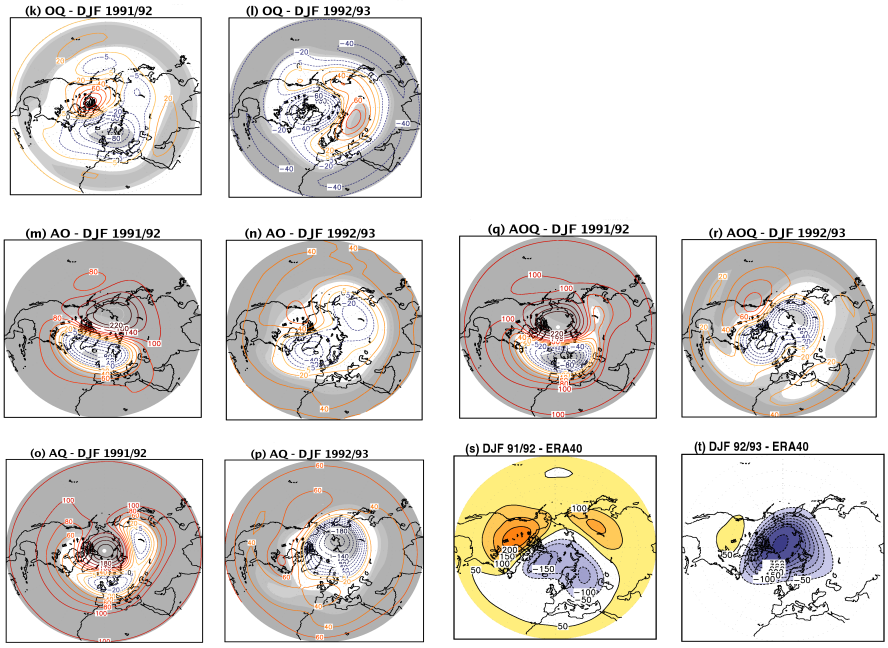

Fig. 4. Continued.

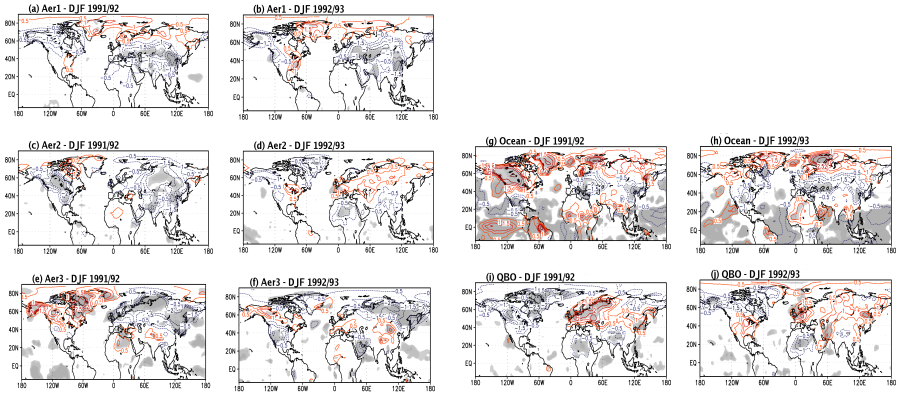

Fig. 5. 2 m temperature anomalies (K) for Aer1 (**a** and **b**); Aer2 (**c** and **d**); Aer3 (**e** and **f**); ocean response (**g** and **h**); qbo response (**i** and **j**); combined ocean and qbo (OQ) (**k** and **l**); combined aerosol and ocean (AO) (**m** and **n**); combined aerosol and QBO (AQ) (**o** and **p**); combined aerosol, ocean and QBO (AOQ) (**q** and **r**); for DJF 1991/1992 (left column) and DJF 1992/1993 (right column). Heavily shaded areas are significant at 99% level, lightly shaded at 90% significance level. Observed 2 m temperature response from ERA-40 (K) for DJF 1991/1992 (**s**) and DJF 1992/1993 (**t**).

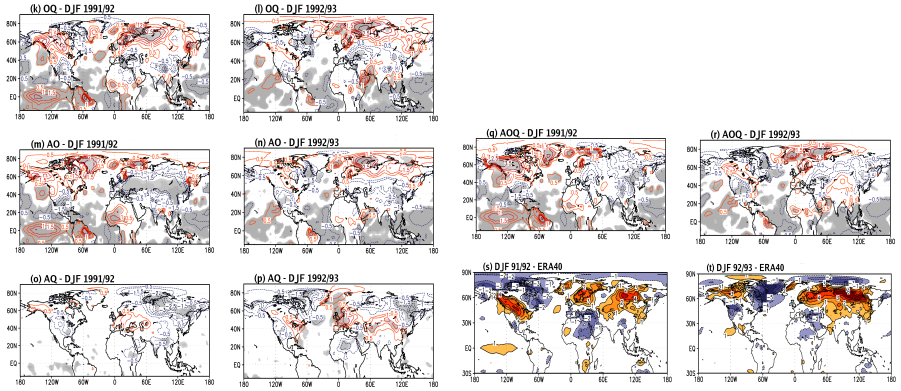

Fig. 5. Continued.